Simultaneous metal-insulator and antiferromagnetic transitions in orthorhombic perovskite iridate Sr_{0.94}Ir_{0.78}O_{2.68} single crystals

H. Zheng, J. Terzic, Feng Ye, X. G. Wan, D. Wang, Jinchen Wang, Xiaoping Wang, P. Schlottmann, S. J. Yuan, and G. Cao

Phys. Rev. B **93**, 235157 — Published 27 June 2016

DOI: 10.1103/PhysRevB.93.235157

Simultaneous Metal-Insulator and Antiferromagnetic Transitions in Orthorhombic Perovskite Iridate $Sr_{0.94}Ir_{0.78}O_{2.68}$ Single Crystals

H. Zheng[1], J. Terzic[1], Feng Ye[2,1], X.G. Wan[3], D. Wang[3], Jinchen Wang[1,2,5], Xiaoping Wang[6], P. Schlottmann[4], S. J. Yuan[1] and G. Cao[1*]

[1]Center for Advanced Materials and Department of Physics and Astronomy
University of Kentucky, Lexington, KY 40506, USA

[2]Quantum Condensed Matter Division, Oak Ridge National Laboratory,
Oak Ridge, TN 37831, USA

[3]Department of Physics, Nanjing University, Nanjing, China

[4]Department of Physics, Florida State University, Tallahassee, FL 32306, USA

[5]Department of Physics, Renmin University of China, Beijing, China

[6]Chemical and Engineering Materials Division, Oak Ridge National Laboratory,
Oak Ridge, TN 37831, USA

The orthorhombic perovskite $SrIrO_3$ is a semimetal, an intriguing exception in iridates where the strong spin-orbit interaction coupled with electron correlations tends to impose a novel insulating state. We report results of our investigation of bulk single-crystal $Sr_{0.94}Ir_{0.78}O_{2.68}$ or Ir-deficient, orthorhombic perovskite $SrIrO_3$. It retains the same crystal structure as stoichiometric $SrIrO_3$ but exhibits a sharp, simultaneous antiferromagnetic (AFM) and metal-insulator (MI) transition occurring in the basal-plane resistivity at 185 K. Above it, the basal-plane resistivity features an extended regime of almost linear-temperature dependence up to 800 K but the strong electronic anisotropy renders an insulating behavior in the out-of-plane resistivity. The Hall resistivity

undergoes an abrupt sign change and grows below 40 K, which along with the Sommerfeld constant of 20 mJ/mole K^2 suggests a multiband effect. All results including our first-principles calculations underscore a delicacy of the paramagnetic, metallic state in $SrIrO_3$ that is in close proximity to an AFM insulating state. The contrasting ground states in isostructural $Sr_{0.94}Ir_{0.78}O_{2.68}$ and $SrIrO_3$ illustrate a critical role of lattice distortions and Ir-deficiency in rebalancing the ground state in the iridates. Finally, the concurrent AFM and MI transitions reveal a direct correlation between the magnetic transition and formation of an activation gap in the iridate, which is conspicuously absent in Sr_2IrO_4.

I. Introduction

It is now widely recognized that strong spin-orbit interaction (SOI) coupled with the electron-electron interaction (on-site Coulomb repulsion U) drives novel narrow-gap Mott insulating states in iridates **[1-7]**. The SOI is a relativistic effect proportional to Z^4 (Z is the atomic number), and is approximately 0.4 eV in the iridates (compared to ~ 20 meV in 3d materials), and splits the t_{2g} bands into states with $J_{eff} = 1/2$ and $J_{eff} = 3/2$, the latter having lower energy in the Ruddlesden-Popper series, $Sr_{n+1}Ir_nO_{3n+1}$ (n = 1 and 2; n defines the number of IrO_6 layers in a unit cell) **[1-7]**. Since Ir^{4+} ($5d^5$) ions provide five 5d-electrons to bonding states, four of them fill the lower $J_{eff} = 3/2$ bands, and one electron partially fills the $J_{eff} = 1/2$ band where the Fermi level E_F resides. The $J_{eff} = 1/2$ band is so narrow that even a reduced U (~ 0.5 eV, due to the extended nature of 5d-electron orbitals) is sufficient to open a small gap Δ supporting the insulating state in $Sr_{n+1}Ir_nO_{3n+1}$. The splitting between the $J_{eff} = 1/2$ and $J_{eff} = 3/2$ bands narrows and the two bands progressively broaden and contribute to the density of states near the Fermi surface as the dimensionality (i.e., n) increases in $Sr_{n+1}Ir_nO_{3n+1}$. In particular, the 5d-bandwidth W of the $J_{eff} = 1/2$ band increases from 0.48 eV for n = 1 to 0.56 eV for n = 2 and 1.01 eV for n = ∞ **[2, 4, 6]**. Since the effects of the SOI and U are largely local and remain essentially unchanged throughout the entire series, $Sr_{n+1}Ir_nO_{3n+1}$, the ground state evolves with decreasing Δ and increasing W , from a robust antiferromagnetic (AFM) insulating state for Sr_2IrO_4 (n = 1) to a paramagnetic semimetallic state for $SrIrO_3$ (n = ∞). That such a semimetallic state occurs in $SrIrO_3$ notwithstanding the presence of the strong SOI is of great interest both theoretically and experimentally **[2, 7-21]**. It is conceived that the strong SOI reduces the threshold of U for a metal-insulator (MI) transition **[8, 9]**. More

recently, theoretical studies find that the stronger SOI requires a larger critical U instead for a MI transition to occur in $SrIrO_3$ because of a protected Dirac node for given U in the J_{eff}=1/2 bands near the Fermi level due to a combined effect of the lattice structure and strong SOI **[10, 11]**. In essence, small hole and electron pockets with a low density of states take place in $SrIrO_3$ and render a less effective U, which would otherwise drive a magnetic insulating state **[10, 11]**. Indeed, tuning the relative strength of the SOI and U effectively changes the ground state in the iridates, and the rare occurrence of a semimetallic state in $SrIrO_3$ provides an unique opportunity to closely examine the intricate interplay of the SOI, U and lattice degrees of freedom. The correlation between the AFM state and MI transition in the iridates has been among the most discussed topics in recent years **[7, 22-24]**.

A good number of excellent studies of the orthorhombic perovskite $SrIrO_3$ have been conducted in recent years **[2, 13-21]**. However, bulk orthorhombic perovskite $SrIrO_3$ forms only at high pressures and high temperatures **[12, 13]**, and almost all studies of $SrIrO_3$ so far are limited to samples in thin-film or polycrystalline form **[2, 13-21]**. Little work on bulk single-crystal $SrIrO_3$ has been reported and critical information, such as anisotropies, magnetic properties and their correlation with the electronic state, etc., is still lacking. (Note that single crystals of the *hexagonal* $SrIrO_3$, which have been studied **[25]**, are not part of this work.) In this paper, we report results of our study on bulk single-crystals of the orthorhombic perovskite $Sr_{0.94}Ir_{0.78}O_{2.68}$ for an extended temperature range from 0.05 K to 800 K. $Sr_{0.94}Ir_{0.78}O_{2.68}$ retains the very same crystal structure as stoichiometric $SrIrO_3$ but exhibits sharp, concurrent AFM and MI transitions at 185 K with a charge gap of 0.027 eV, sharply contrasting with stoichiometric $SrIrO_3$ that is

paramagnetic and semimetallic. The electrical resistivity is highly anisotropic and features an extended regime of approximately linear-T basal-plane resistivity between 185 K and 800 K. The Hall resistivity undergoes an abrupt sign change near 40 K (rather than at T_N=185 K), from holelike at high temperatures to electronlike at low temperatures, which along with a finite Sommerfeld constant of 20 mJ/mole K^2 implies in-gap states. Our band structure calculations confirm a small energy gap and finite magnetic moment in an AFM insulating state as a result of the Ir deficiencies in $Sr_{0.94}Ir_{0.78}O_{2.68}$. This work underscores the delicacy of the metallic state that is in close proximity to an AFM insulating state that is highly sensitive to even slight lattice defects in $SrIrO_3$. The concurrent AFM and MI transitions provide clear evidence for a direct correlation between the magnetic transition and charge gap in $SrIrO_3$, which is absent in Sr_2IrO_4.

II. Experimental details

The single crystals studied were grown at ambient pressure from off-stoichiometric quantities of $SrCl_2$, $SrCO_3$ and IrO_2 using self-flux techniques. The mixed powders with a weight ratio of Sr to Ir being 4 to 1 were fired up to 1470 ^oC for 5 hours and then slowly cooled down at a rate of 2 ^oC/hour. The size of the single crystals is of 1.0x0.5x0.5 mm^3. The formation of nonstoichiometric $SrIrO_3$ single crystals at ambient pressure is consistent with recent observations that the orthorhombic perovskite phase can be stabilized at ambient pressure via chemical doping **[13-16]**. The crystal structure of single-crystal $Sr_{0.94}Ir_{0.78}O_{2.68}$ was determined using a Rigaku X-ray diffractometer XtaLAB PRO equipped with PILATUS 200K hybrid pixel array detector at the Oak Ridge National Laboratory. More than 20 crystals were carefully examined. Full data sets

were collected from 100 K to 260 K and the structures were refined using SHELX-97 and FullProf software **[26, 27]** (see **Table 1**). Chemical compositions of single-crystal $Sr_{0.94}Ir_{0.78}O_{2.68}$ were determined using energy dispersive X-ray analysis (EDX) (Hitachi/Oxford 3000) and X-ray diffraction discussed below. Magnetization, specific heat, Hall and electrical resistivity were measured using either a Quantum Design MPMS-7 SQUID Magnetometer and/or Physical Property Measurement System with 14-T field capability. The Hall resistivity as functions of temperature or magnetic field was determined by the difference between two sets of transverse resistivity data taken at a magnetic field with the same magnitude but opposite directions. AC resistance bridges (Linear Research 700 and Lakeshore 370) were used for transport measurements. The high-temperature resistivity was measured using a Displex closed cycle cryostat capable for a continuous temperature ramping from 9 K to 900 K.

The electronic band structure calculations were performed using the full potential linearized augmented plane wave method as implemented in WIEN2K package. Local spin density approximation (LSDA) for the exchange-correlation potential was used. We utilized an LSDA+SOI+U (U = 3 eV) scheme. The self-consistent calculations were considered converged when the difference in the total energy of the crystal does not exceed 0.01 mRy.

III. Crystal structure

The single-crystal $Sr_{0.94}Ir_{0.78}O_{2.68}$ adopts an orthorhombic perovskite structure with space group *Pbnm* (No. 62), as shown in **Fig. 1** and **Table. 1**. It has 3.12 Ir atoms, rather than 4, in a unit cell but its crystal structure is consistent with that of stoichiometric, orthorhombic perovskite $SrIrO_3$ reported in literature **[12-17]**. The Ir and

O deficiencies inevitably lead to proportionally smaller lattice parameters of $Sr_{0.94}Ir_{0.78}O_{2.68}$ than those of $SrIrO_3$ with an approximate 2.5% decrease in volume (for the high-pressure bulk $SrIrO_3$ phase**,** a = 5.60075 (5.58871) Å, b = 5.57115 (5.57245) Å, c = 7.89601 (7.88413) Å, and V = 246.376 (245.534) $Å^3$ at 300 K (3 K) **[17])**. The Ir-O-Ir bond angles for in-plane and out-of-plane are 161.1 (3)^o and 162.3 (4)^o, respectively. A close comparison with the data of the stoichiometric $SrIrO_3$ in Ref. 17 indicates that $Sr_{0.94}Ir_{0.78}O_{2.68}$ has a larger in-plane rotation of IrO_6 octahedra, 9.54^o (vs. 8.75^o) but a smaller out-of-plane tilt, 8.85^o (vs. ~12^o). The in-plane rotation is likely to have a greater impact on physical properties than the out-of-plane tilt. Note that the IrO_6 octahedra in Sr_2IrO_4 and $Sr_3Ir_2O_7$ only rotate within the basal plane by about 12^o without the out-of-plane tilt **[28-31]**.

Table 1. **Structural parameters for single-crystal perovskite $Sr_{0.94}Ir_{0.78}O_{2.68}$ at 150K**

T = 150 K	*The lattice parameters*: ***a* = 5.541(6) Å, *b* = 5.535(5) Å, *c* = 7.833(8) Å,** and **V = 240.3(4) $Å^3$**; *Space group*: ***Pbnm* (No. 62)**. The agreement factor R_1 = 4.33% was achieved by using 392 unique reflections with I > 4σ and resolution of d_{min} =0.65 Å. Anisotropic atomic displacement parameters were used for all elements involved.					
	Site	x	y	z	Occupancy	Ueq($Å^2$)
Sr1	4c	0.0029(2)	0.5094(2)	0.25	0.94(3)	0.0174(5)
Ir2	4c	0.0029(2)	0.5094(2)	0.25	0.06(3)	0.0174(5)
Ir1	4a	0	0	0	0.72(3)	0.0086(3)
O1	4c	-0.067 (2)	-0.004(1)	0.25	1	0.022(3)
O2	8d	0.232(1)	0.268(2)	0.035(1)	0.84(4)	0.022(2)

In addition, the crystal structure is also systematically examined in a temperature range of 100 K - 260 K using single crystal x-ray diffraction. No lattice anomaly is discerned in this temperature range including 185 K where AFM and MI transitions occur, which is discussed below.

IV. Experimental results

A. Magnetic properties

One of the central features of $Sr_{0.94}Ir_{0.78}O_{2.68}$ is that a robust AFM transition occurring at T_N=185 K (**Fig.2a**) is accompanied by a sharp MI transition. Fitting the a-axis magnetic susceptibility $\chi_a(T)$ in **Fig. 2a** to a Curie-Weiss law for 200-340 K yields the Curie-Weiss temperature θ_{CW} = +160 K and the effective moment μ_{eff} = 0.19 μ_B/Ir. Like that of Sr_2IrO_4 and other related iridates **[4, 32, 33]**, θ_{CW} show a characteristic positive sign, despite the AFM ground state. μ_{eff} is finite but significantly smaller than that for other more insulating iridates (*e.g.*, 0.4 μ_B/Ir for Sr_2IrO_4) due to the more itinerant nature of the system discussed below. The isothermal magnetization M(H) varies almost linearly with the magnetic field H up to 7 T, as anticipated for an AFM ground state (see **Fig.2b**). The magnetic anisotropy is visible but weak, consistent with the nature of the orthorhombic perovskite. For comparison, the evolution of the AFM order in the Ruddlesden-Popper series $Sr_{n+1}Ir_nO_{3n+1}$ with n=1, 2 and $Sr_{0.94}Ir_{0.78}O_{2.68}$ (n=∞) is illustrated in **Fig. 2c**. T_N for $Sr_{0.94}Ir_{0.78}O_{2.68}$ is clearly lower than that for n=1 (240 K) and n=2 (285 K) but the low-temperature magnetic moment of $Sr_{0.94}Ir_{0.78}O_{2.6}$ seems considerably stronger than that of n=2 (right scale in **Fig.2c**).

B. Electrical resistivity

The electrical resistivity ρ(T) features a sharp MI transition at T_N =185 K and an almost linear-T dependence of the a-axis ρ_a for an extended regime of 185 K-800 K. Along the c-axis, the apparent electronic anisotropy leads to a much less metallic behavior or in which ρ_c, with much weaker temperature dependence above T_N, is more than one order of magnitude greater than ρ_a despite the nearly isotropic structure (see **Fig.3a**). It is remarkable that the system exhibits a metallic character within the basal

plane but insulating behavior out-of-plane above T_N. The c-axis ρ_c fits perfectly an activation law, $\rho_c \sim \exp(\Delta/T)$, for 125 K <T < 350 K; an evident slope change at T_N signals a significant widening of the activation gap Δ from 0.008 eV above T_N to 0.027 eV below T_N (see **Inset** in **Fig.3a**). ρ_c does not follow any power law below 125 K. The occurrence of the sharp MI transition at T_N with the pronounced change of Δ clearly indicates a strong correlation between the AFM and MI transitions in this iridate. This behavior sharply contrasts with that of Sr_2IrO_4 in which such a correlation seems more intricate, unconventional and still open to debate **[22, 23]**. Furthermore, ρ_a exhibits the metallic behavior above T_N, which would suggest a Slater transition; however, ρ_c indicates that the insulating state already exists above T_N, which seems to be consistent with a Mott transition. This peculiar feature is absent in other iridates. In fact, the distinct temperature dependence of ρ_a and ρ_c above T_N seems similar to that for so-called strange metals, which is observed in the ruthenates **[34]** and cuprates **[35, 36]**.

An extended regime of linear temperature resistivity is a classic signature of high-T_C cuprates and the p-wave superconductor Sr_2RuO_4, Fe-based superconductors and many other correlated oxides **[37]**, in which spin fluctuations play an important role in the electron scattering. Elementary Bloch-Grüneisen theory predicts $\rho(T) \sim T$ for $T >> \theta_D$, in the case of electron-phonon scattering where Debye temperature θ_D = 343 K for $Sr_{0.94}Ir_{0.78}O_{2.68}$. Resistivity saturation is anticipated when the mean-free path *l* of the quasiparticles becomes shorter than the lattice parameter *a* (Mott-Ioffe-Regel limit **[38, 39]**), or for $\rho \sim$ 100-150 $\mu\Omega$ cm (Mooij limit, **[40, 41]**). Here $\rho_a(T)$ for $Sr_{0.94}Ir_{0.78}O_{2.68}$ is well above the Mott-Ioffe-Regel or Mooij limits, and yet shows no sign of saturation up to 800 K. Furthermore, both $\rho_a(T)$ and $\rho_c(T)$ show an anomaly near T*=40 K that

accompanies no corresponding magnetic anomaly. The origin of T* is unclear but closely related to the Hall resistivity discussed below.

For comparison and contrast, ρ_a for $Sr_{n+1}Ir_nO_{3n+1}$ with n=1, 2 and $Sr_{0.94}Ir_{0.78}O_{2.68}$ (n=∞) is presented in **Fig. 3b**. ρ_a decreases rapidly by as much as seven orders of magnitude at low temperatures as n increases from n=1 to n=∞, and the ground state evolves from the insulating state at n=1 to a much more metallic state at n=∞, particularly above T_N.

C. Hall resistivity

The Hall resistivity $\rho_H(T)$ is linear in the magnetic field up to 7 T (see inset of **Fig. 3c**). $\rho_H(T)$ taken at μ_oH=7 T for $Sr_{0.94}Ir_{0.78}O_{2.68}$ exhibits an abrupt change in temperature dependence near T*, marking a drop in $\rho_H(T)$, thus a sign change from positive to negative with decreasing temperature, suggesting a multiband effect (**Fig. 3c)**. It appears that holes as charge carriers predominate above T* whereas electrons become overwhelming below T*. The sign change is probably due to a change with temperature of the mobilities (two-band model). A two-carrier type model (p and n) needs to be considered to adequately determine the carrier densities but a rough estimate using the Drude theory yields the carrier densities to be of order of $10^{19}/cm^3$. $Sr_{0.94}Ir_{0.78}O_{2.68}$ is electron doped by 0.36 electrons per unit formula. It is likely that most of the electrons are trapped by disorder scattering and do not contribute to the Hall resistivity. It is also worth pointing out that the Hall resistivity of this compound is much larger than that in $SrIrO_3$ **[20, 21]**, possibly suggesting a departure from the nearly compensate character of $SrIrO_3$. This indicates that the severe off-stoichiometry of this compound actually provides charge doping.

D. Heat capacity

The specific heat C(T) was measured over an extended range, 0.05 K < T < 250 K. A slope change in C(T) occurs near T_N, confirming the magnetic phase transition (see **Fig. 4a**). C(T) for 1 K < T < 4 K approximately fits the common expression, $C(T) = \gamma T + \beta T^3$, where the first term arises from the electronic contribution to C(T) and the second term the phonon contribution; γ is usually a measure of the density of states of the conduction states near the Fermi surface and effective mass, however, localized states or tunneling of atoms in a double well potential can also contribute to γ. β is related to the Debye temperature θ_D, which for this iridate is 343 K but can also include a contribution from antiferromagnetic spinwaves (**Fig.4b**). Despite the nonmetallic ground state, γ of this iridate is estimated to be 20 mJ/mole K^2 at $\mu_o H$=0 T, suggesting that the finite density of states near the Fermi level arises from localization due to disorder. Interestingly, γ is significantly greater than the 3 mJ/mole K^2 for stoichiometric $SrIrO_3$ **[17]**, this is in part due to localized electrons.

Furthermore, C(T) at low temperatures changes sensitively at relatively low magnetic field H, particularly below 1 K, as illustrated in **Fig. 4b** where C/T varies drastically with H. The approximate fitting of the data in **Fig.4b** to $C(T)/T = \gamma + \beta T^2$ for 0.05 K < T < 1 K generates γ as a function of H as shown in **Fig. 4c**. γrises pronouncedly from 20 mJ/mole K^2 at $\mu_o H$=0 T to 41 mJ/mole K^2 at $\mu_o H$=2 T before decreasing with increasing H. The origin of the unusual field-dependence of γ is unclear but it could be due to in-gap states and/or a field-induced magnetic order that shifts up to higher temperature with increasing H (**Fig.4b**). It is not unusual for strongly correlated electron systems that the expression $\gamma T + \beta T^3$ fit does not continue down to 0 K. This is common

for heavy fermion compounds and implies a change of mechanism at very low temperatures.

V. Band Structure

Our first-principles calculations for both $Sr_{0.94}Ir_{0.78}O_{2.68}$ and stoichiometric $SrIrO_3$ using the LSDA+SOI+U method with U=3eV result in different band topologies (**Figs. 5a** and **5b**). The octahedral crystal field splits the bands into e_g and t_{2g}-like orbitals. The bands closest to the Fermi level are t_{2g}-orbitals hybridized with O. The band structure for $SrIrO_3$ is in agreement with that reported in **Ref. 10** (**Fig.5b**).

For $Sr_{0.94}Ir_{0.78}O_{2.68}$, we use a supercell of $Sr_8Ir_6O_{22}$, which is sufficiently close to $Sr_{0.94}Ir_{0.78}O_{2.68}$ and corresponds to two cells as shown in **Fig. 5c**. There are three Ir ions in each cell with different local environments due to the O coordination and tilting and rotations of the octahedra. According to the calculations, the Ir- and O-deficiencies alter the IrO_6 octahedra, leading to three distinct Ir sites denoted by A, B and C in **Fig. 5c**. For site A the IrO_6 octahedra remain intact, and for site B the IrO_6 octahedra remain but with a broken Ir-O-Ir bond along the c- or z-direction, and for the site C, the IrO_6 octahedra evolve to IrO_5 prisms because of a missing O (**Fig. 5c**). Note that the tilting and rotations of Ir-O octahedra occur in all three sites. For the site A, J_{eff}=3/2 and J_{eff}=1/2 states with a magnetic moment of 0.19 μ_B/Ir are anticipated; for the site B, the broken Ir-O-Ir bond along the z-direction renders a fully occupied d_{xy} orbital (the lowest state) and half-filled d_{yz}, and d_{xz} orbitals. Thus, as shown in **Fig. 5d**, the electrons can easily hop between the sites A and B, which would explain metallic behavior in the basal plane. The J_{eff}=3/2 and J_{eff}=1/2 states arise from the combined effect of the SOI and the cubic crystalline electric field. The broken Ir-O-Ir bond gives rise to a tetragonal crystal field which is usually

larger than a cubic one and competes with the SOI so that the J_{eff}=3/2 and J_{eff}=1/2 states are not formed at the site B. Similarly, for the site C a tetragonal crystalline field develops and the d_{yz}, and d_{xz} orbitals are fully occupied, which favors an insulating behavior along the c-direction, as indeed indicated in the electrical resistivity (**Fig.3a**). The band calculations (**Fig. 5a**) illustrate an insulating ground state in $Sr_{0.94}Ir_{0.78}O_{2.68}$ that emerges from a metallic state in $SrIrO_3$ as the Ir and O deficiencies break some pathways of electron hopping along the c-axis in $Sr_{0.94}Ir_{0.78}O_{2.68}$. A narrow charge gap of 0.081 eV for $Sr_{0.94}Ir_{0.78}O_{2.68}$ is predicted, which is somewhat larger but qualitatively consistent with 0.027 eV estimated from ρ_c below T_N or for 125 < T < 185 K.

In essence, the Ir- and O-deficiencies generate the three distinct Ir sites and it is this differences between them that induces the unexpected anisotropic resistivity (**Fig. 3a**), despite the near cubic structure of $Sr_{0.94}Ir_{0.78}O_{2.68}$. It is worth mentioning that the rotation of IrO_6 octahedra within the basal plane is a structural signature of Sr_2IrO_4 and $Sr_3Ir_2O_7$ **[28-31]** and is critical to the AFM ground state **[42]**. The AFM state in $Sr_{0.94}Ir_{0.78}O_{2.68}$ might be in part a result of the increased in-plane rotation of IrO_6 octahedra, 9.54^o (compared to 8.75^o for $SrIrO_3$) whereas the decreased out-of-plane tilt, which is absent in n=1 and 2, may not be as critical in determining the ground state.

The supercell considered here is only a first order approximation to the real compound. Normalizing $Sr_{0.94}Ir_{0.78}O_{2.68}$ to 6 Ir ions we have 7.23 Sr atoms and 20.62 O atoms per supercell. This differs somewhat from $Sr_8Ir_6O_{22}$ and it is therefore necessary to consider a much larger supercell to obtain a more precise band structure with the correct

composition. On the other hand, this is only the average composition and one should allow for some fluctuations in the composition. A few details of the calculations need more clarity: No assumption that oxygen vacancies surround the Ir vacancies was made in the calculations. Instead, several possible states were assumed and optimized in order to identify the one having the lowest total-energy. The atomic positions were optimized in the calculations. For the site A, IrO_6 octahedra hardly change. For the site B, the broken Ir-O-Ir bonds along the c-axis reduces the apical Ir-O bonds. For the site C, the oxygen vacancy changes the IrO_5 prisms to trigonal bipyramidal.

VI. Conclusion

This work reveals the simultaneous AFM and MI transitions that illustrate a direct correlation between the AFM transition and charge gap in the iridate, which is conspicuously absent in Sr_2IrO_4. The contrasting ground states in isostructural $Sr_{0.94}Ir_{0.78}O_{2.68}$ and $SrIrO_3$ highlight the critical role of the lattice degrees of freedom that along with the delicate interplay of the SOI and U needs to be adequately addressed both experimentally and theoretically. In particular, the elusive superconductivity in the iridates, despite the apparent similarities between the cuprates and iridates, might be in part due to the ultra-high sensitivity to lattice distortions in the SOI-coupled iridates; the lattice-dependence in the cuprates is much weaker since the SOI, which anchors physical properties to the lattice in general, is negligible.

Acknowledgements GC is very thankful for enlightening conversations with Profs. Hae-Young Kee and Yong-Baek Kim. This work was supported by NSF through grant DMR-1265162 0856234 and the Department of Energy (BES) through grant No. DE-FG02-

98ER45707 (PS). G.W. acknowledges support by Natural Science Foundation of China via Grant No.11525417.

* Email: cao@uky.edu

References

1. B. J. Kim, Hosub Jin, S. J. Moon, J.-Y. Kim, B.-G. Park, C. S. Leem, Jaejun Yu, T. W. Noh, C. Kim, S.-J. Oh, V. Durairai, G. Cao, and J.-H. Park, Phys. Rev. Lett. **101**, 076402 (2008)
2. S.J. Moon, H. Jin, K.W. Kim, W.S. Choi, Y.S. Lee, J. Yu, G. Cao, A. Sumi, H. Funakubo, C. Bernhard, and T.W. Noh, Phys. Rev. Lett. **101**, 226402 (2008)
3. B.J. Kim, H. Ohsumi, T.Komesu, S.Sakai, T. Morita, H. Takagi, T. Arima, Science **323**, 1329 (2009)
4. *"Frontiers of 4d- and 5d- Transition Metal Oxides"*, Gang Cao and Lance E. De Long, *World Scientific*, Singapore, 2013
5. William Witczak-Krempa, Gang Chen, Yong Baek Kim, Leon Balents, Annual Review of Condensed Matter Physics, Vol. 5: 57-82 (2014)
6. Q. Wang, Y. Cao, J. A. Waugh, T. F. Qi, O. B. Korneta, G. Cao, and D. S. Dessau, *Phys. Rev B* **87** 245109 (2013)
7. Jeffrey G. Rau, Eric Kin-Ho Lee, and Hae-Young Kee, Annu. Rev. Condens. Matter Phys 7, 195 (2016)
8. D. Pesin and L. Balents, Nat. Phys. 6, 376 (2010)
9. H. Watanabe, T. Shirakawa and S. Yunoki, Phys. Rev. Lett. 105, 216410 (2010)
10. M. Ahsan Zeb and Hae-Young Kee, Phys. Rev. B 86, 085149 (2012)

11. Yige Chen Yuan-Ming Lu Hae-Young Kee, Nature Comm. doi:10.1038/ncomms7593 (2015)
12. J. M. Longo, J. A. Kafalas and R. J. Arnott, J. Solid State Chem., **3**, 174 (1971)
13. J. G. Zhao, L. X. Yang, Y. Yu, F. Y. Li, R. C. Yu, Z. Fang, L. C. Chen, and C. Q. Jin, J. Appl. Phys., **103**, 103706 2008
14. M. Bremholm, C. K. Yim, D. Hirai, E. Climent-Pascual, Q. Xu, H. W. Zandbergen, M. N. Ali and R. J. Cava, J. Mater. Chem., **22**, 16431 (2012)
15. I. Qasim, B. J. Kennedy and M. Avdeev, J. Mater. Chem. A, **1**, 3127 (2013)
16. I. Qasim, B. J. Kennedy, and M. Avdeev, J. Mater. Chem. A, **1**, 13357 (2013)
17. P. E. R. Blanchard, E. Reynolds, and B. J. Kennedy, Phys. Rev. B **89**, 214106 (2014)
18. John H. Gruenewald, John Nichols, Jasminka Terzic, Gang Cao, Joseph W. Brill, and Sung S. Ambrose Seo, J. Mater. Res. **29**, 2495 (2014)
19. Y.□F. Nie, P.□D.□C. King, C.□H. Kim, M. Uchida, H.□I. Wei, B.□D. Faeth, J.□P. Ruf, J.□P.□C. Ruff, L. Xie, X. Pan, C.□J. Fennie, D.□G. Schlom, and K.□M. Shen, Phys. Rev. Lett. **114**, 016401 (2015)
20. J. Matsuno, K. Ihara, S. Yamamura, H. Wadati, K. Ishii, V.□V. Shankar, Hae-Young Kee, and H. Takagi, Phys. Rev. Lett. **114**, 247209 (2015)
21. J. Liu, J. H. Chu, C. R. Serrao, D. Yi, J. Koralek, C. Nelson, C. Frontera, D. Kriegner, L. Horak, E. Arenholz et al., arXiv:1305.1732, 2013
22. D. Hsieh, F. Mahmood, D. Torchinsky, G. Cao and N. Gedik, *Phys. Rev. B* **86**, 035128 (2012)

23. Q. Li, G. Cao, S. Okamoto, J. Yi, W. Lin, B.C. Sales, J. Yan, R. Arita, J. Kuneš, A.V. Kozhevnikov, A.G. Eguiluz, M. Imada, Z. Gai, M. Pan, D.G. Mandrus, *Scientific Reports* 3, 3073 (2013)

24. J. C. Wang, S. Aswartham, F. Ye, J. Terzic, H. Zheng, Daniel Haskel, Shalinee Chikara, Yong Choi, P. Schlottmann, S. J. Yuan[1] and G. Cao, *Phys. Rev. B* ***92***, 214411 (2015)

25. G. Cao, V. Durairaj, S. Chikara, L. E. DeLong, S. Parkin, and P. Schlottmann, Phys. Rev. B **76**, 100402(R) (2007)

26. G. M. Sheldrick, Acta Crystallogr A **64**, 112 (2008)

27. J. Rodriguez-Carvajal, Physica B. **192,** 55 (1993)

28. M.K. Crawford, M.A. Subramanian, R.L. Harlow, J.A. Fernandez-Baca, Z.R. Wang, and D.C. Johnston, Phys. Rev. B **49**, 9198 (1994)

29. R.J. Cava, B. Batlogg, K. Kiyono, H. Takagi, J.J. Krajewski, W. F. Peck, Jr., L.W. Rupp, Jr., and C.H. Chen, Phys. Rev. B **49**, 11890 (1994)

30. M.A. Subramanian, M.K. Crawford, R. L. Harlow, T. Ami, J. A. Fernandez-Baca, Z.R. Wang and D.C. Johnston, Physica C **235**, 743 (1994)

31. G. Cao, Y. Xin, C. S. Alexander, J.E. Crow and P. Schlottmann, *Phys. Rev. B* 66, 214412 (2002)

32. G. Cao, J. Bolivar, S. McCall, J.E. Crow, and R. P. Guertin, Phys. Rev. B **57**, R11039 (1998)

33. G. Cao, J.E. Crow, R.P. Guertin, P. Henning, C.C. Homes, M. Strongin, D.N. Basov, and E. Lochner, *Solid State Comm.* 113, 657 (2000)

34. A. W. Tyler and A. P. Mackenzie, S. NishiZaki and Y. Maeno, Phys. Rev. B 58, R10107 (1998)

35. T. Watanabe, T. Fujii, and A. Matsuda, Phys. Rev. Let. 79, 2113 (1997)

36. B. Bucher, P. Stainer, J. Karpinski, E. Kildis, P. Wachter, Phys. Rev. Lett. 70, 2012 (1993)

37. G. Cao, W.H. Song, Y.P. Sun and X.N. Lin, *Solid State Comm.* **131**, 331 (2004)

38. J. H. Mooij, *Phys. Status Solidi* A **17**, 521 (1973)

39. C. A. Balseiro and L. M. Falicov, *Phys. Rev. B* **20**, 4457 (1979)

40. A. M. Gabovich, A. I. Voitenko, T. Ekino, M. S. Li, H. Szymczak, and M. Pekala, *Adv. Cond. Matter Phys.* **2010**, 681070 (2010)

41. M. Weger and N.F. Mott, *J. Phys. C: Solid St. Phys*. **18**, L201 (1985)

42. G. Jackeli and G. Khaliulin, Phys. Rev. Lett. **102**, 017205 (2009)

Captions

Fig. 1. The crystal structure of perovskite $Sr_{0.94}Ir_{0.78}O_{2.68}$. Legends: green: Sr, brown: Ir, and red: Oxygen. Note there are 3.08 Ir atoms in a unit cell, as compared to 4 in $SrIrO_3$.

Fig. 2. (a) The temperature dependence at μ_oH=0.5 T of the magnetic susceptibility χ for a-axis χ_a and c-axis χ_c, and χ_a^{-1} (right scale) for $Sr_{0.94}Ir_{0.78}O_{2.68}$. **(b)** The isothermal magnetization M_a (blue) and M_c (red) up to 7 Tesla. **(c)** The temperature dependence of χ_a for $Sr_{n+1}Ir_nO_{3n+1}$ with n=1, 2 and ∞. Note θ_{CW} and μ_{eff} are the Curie-Weiss temperature and effective moment, respectively.

Fig. 3. The temperature dependence of **(a)** the a-axis resistivity ρ_a and the c-axis resistivity ρ_c for $Sr_{0.94}Ir_{0.78}O_{2.68}$, (note that ρ_c is on a logarithmic scale on the right axis), **(b)** ρ_a for $Sr_{n+1}Ir_nO_{3n+1}$ with n=1, 2 and ∞, and **(c)** the Hall resistivity ρ_H for $Sr_{0.94}Ir_{0.78}O_{2.68}$. **Inset** in **(a)**: ln ρ_c vs. T^{-1}. **Inset** in **(c)**: the magnetic field dependence of ρ_H at a few representative temperatures.

Fig. 4. (a) The specific heat C(T) for 100 <T<250 K. **(b)** C(T)/T vs. T^2 for 1<T<4 K at a few representative magnetic fields. **(c)** C(T)/T or γ vs. μ_oH for $Sr_{0.94}Ir_{0.78}O_{2.68}$.

Fig. 5. Comparisons of the band structures calculations using LSDA+U+SO (U=3 eV) for **(a)** $Sr_{0.94}Ir_{0.78}O_{2.68}$ and **(b)** stoichiometric $SrIrO_3$; the Fermi level is at 0. Note that the energy range, -3.0 to 1.0 eV, is dominated by Ir 5d states whereas the 2p states of O are located below -2.0 eV**.** The crystal fields of the sites A, B and C are different from one another and there is strong hybridization between them; the bands cannot be labeled distinctly in the figure. **(c)** The schematic structure for $Sr_{0.94}Ir_{0.78}O_{2.68}$ illustrates three different Ir ion sites due to the non-stoichiometry: A ($5d^5$), B ($5d^4$) and C ($5d^4$) (see text), and **(d)** the corresponding 5d-orbitals and electron hopping between the orbitals.

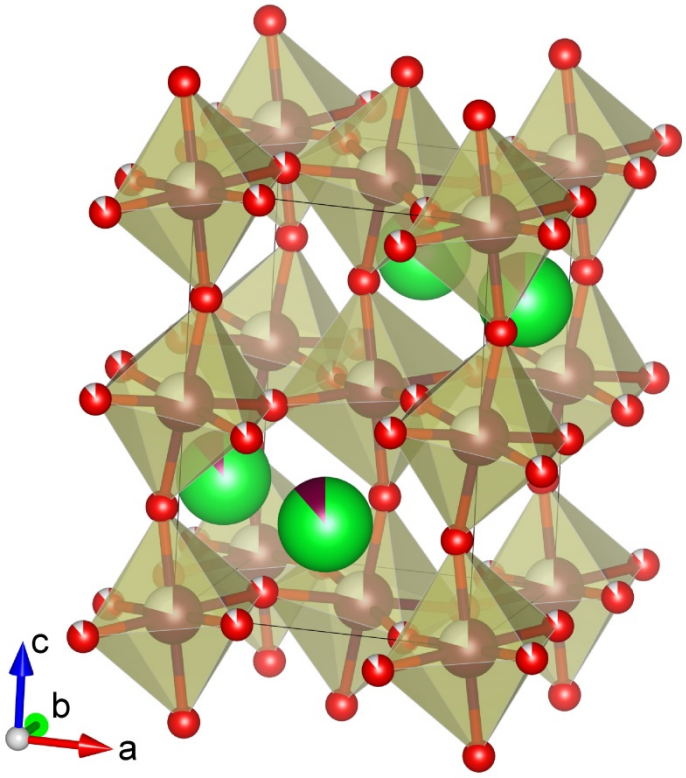

Fig.1

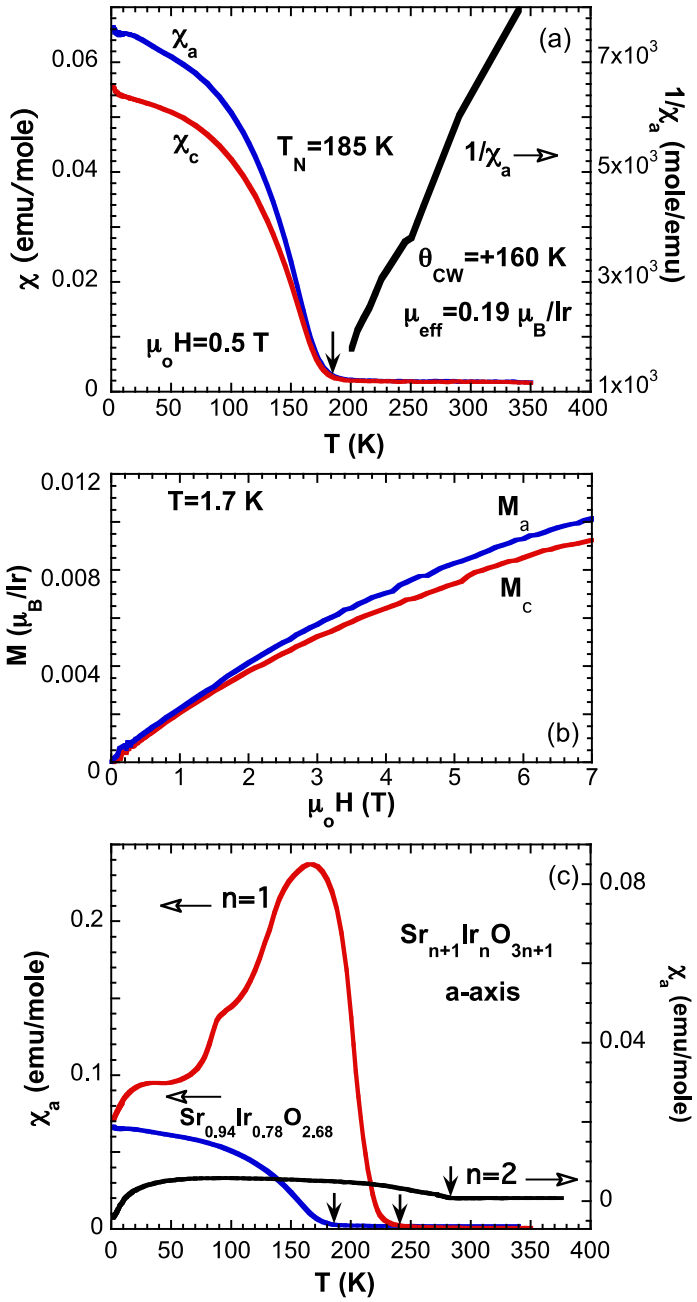
(a)
χa
χc
TN=185 K
1/χa
θCW=+160 K
μeff=0.19 μB/Ir
μoH=0.5 T
χ (emu/mole)
1/χa (mole/emu)
T (K)
(b)
T=1.7 K
Ma
Mc
M (μB/Ir)
μoH (T)
(c)
n=1
Sr n+1 Ir n O 3n+1
a-axis
Sr0.94Ir0.78O2.68
n=2
χa (emu/mole)
χa (emu/mole)
T (K)

Fig. 2

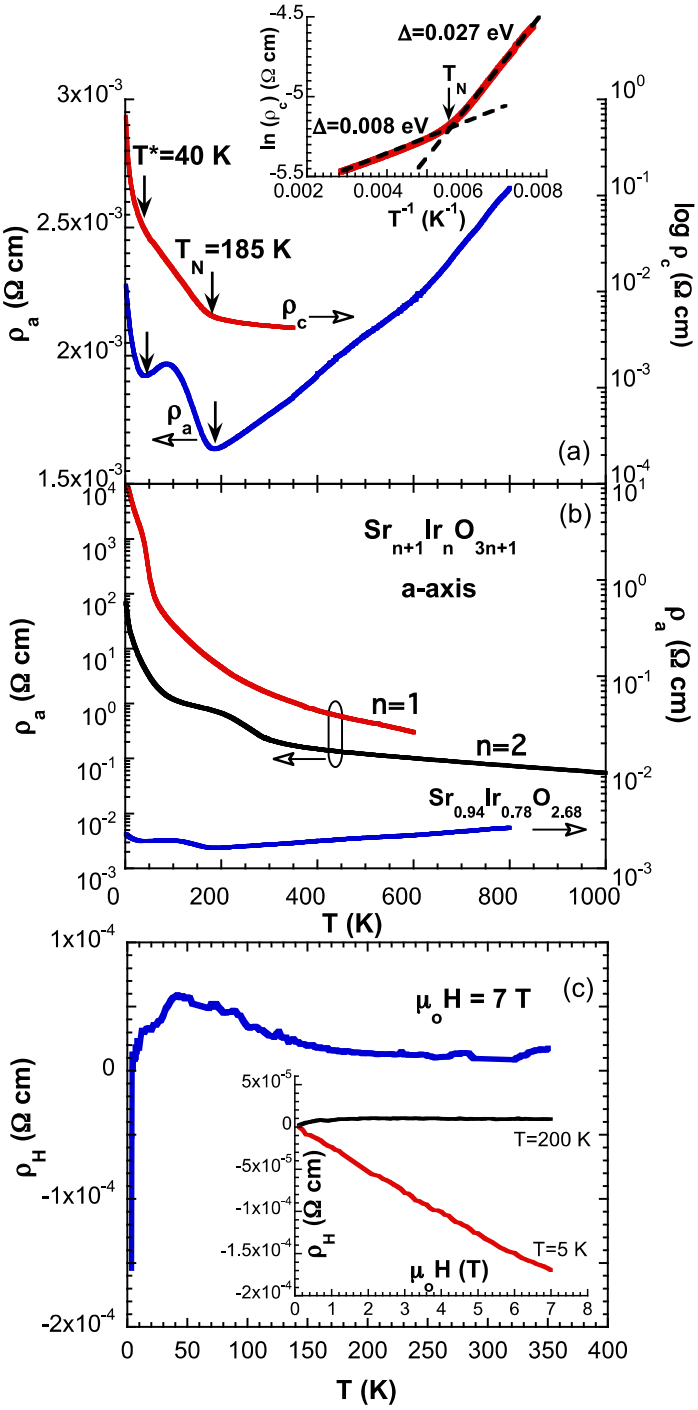
Δ=0.027 eV
T_N
Δ=0.008 eV
ln (ρ_c) (Ω cm)
T^-1 (K^-1)
T*=40 K
T_N=185 K
ρ_c
ρ_a
ρ_a (Ω cm)
log ρ_c (Ω cm)
(a)
(b)
Sr_n+1 Ir_n O_3n+1
a-axis
n=1
n=2
Sr_0.94 Ir_0.78 O_2.68
ρ_a (Ω cm)
ρ_a (Ω cm)
T (K)
μ_o H = 7 T
(c)
T=200 K
T=5 K
ρ_H (Ω cm)
μ_o H (T)
ρ_H (Ω cm)
T (K)

Fig. 3

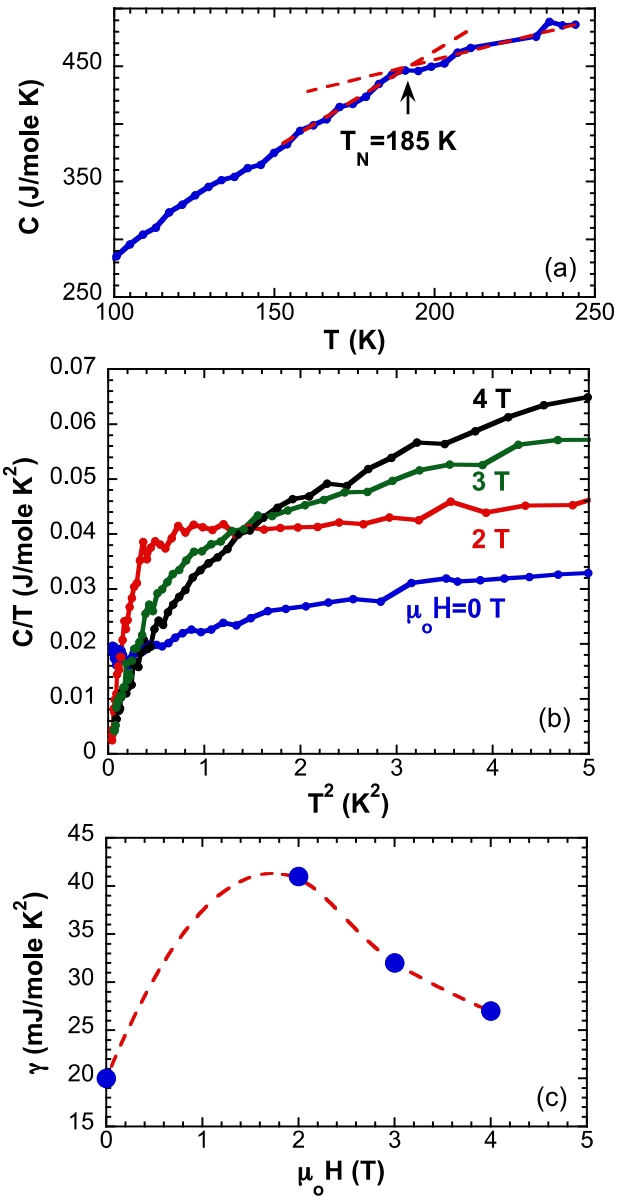
C (J/mole K)
450
350
250
100
150
200
250
T (K)
T_N=185 K
(a)
C/T (J/mole K^2)
0.07
0.06
0.05
0.04
0.03
0.02
0.01
0
0
1
2
3
4
5
T^2 (K^2)
4 T
3 T
2 T
μ_o H=0 T
(b)
γ (mJ/mole K^2)
45
40
35
30
25
20
15
0
1
2
3
4
5
μ_o H (T)
(c)

Fig. 4

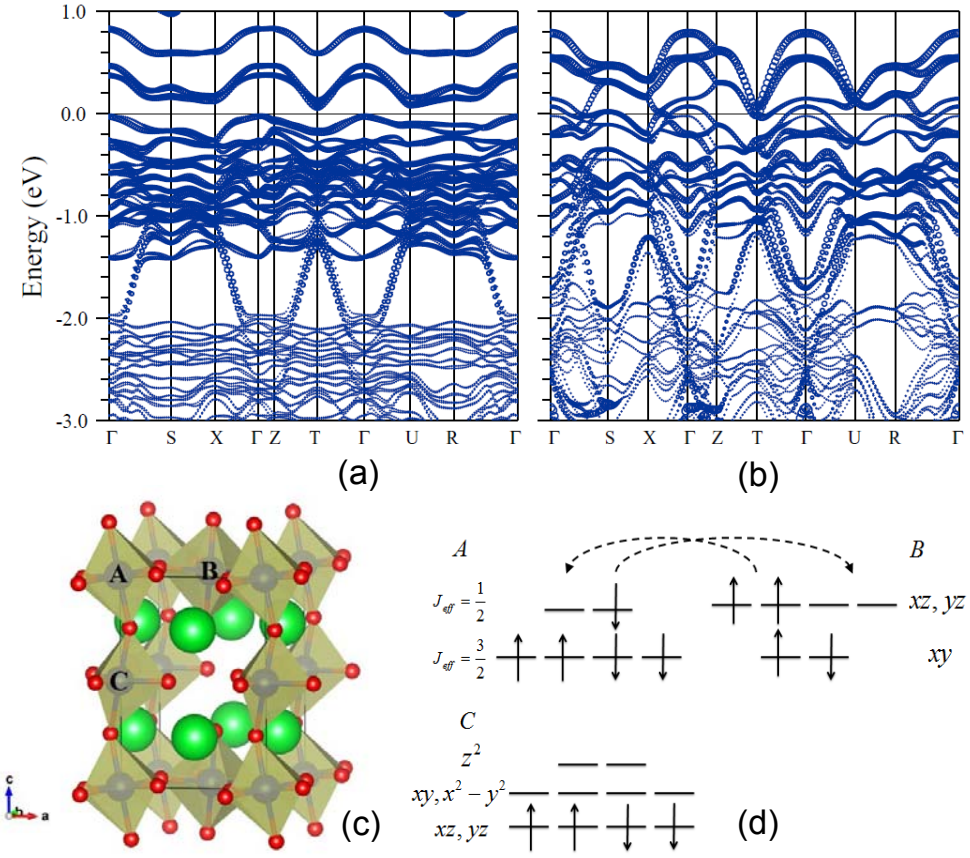
1.0
0.0
-1.0
-2.0
-3.0
Energy (eV)
Γ S X Γ Z T Γ U R Γ
(a)
(b)
A
B
C
c
b
a
(c)
A
B
$J_{eff} = \frac{1}{2}$
$J_{eff} = \frac{3}{2}$
xz, yz
xy
C
z^2
$xy, x^2 - y^2$
xz, yz
(d)

Fig.5